
Tokyo Gakugei University Repository
東京学芸大学リポジトリ
http://ir.u-gakugei.ac.jp/

Title	Graded persisting activity of heterogeneous neuron ensembles subject to white noises
Author(s)	長谷川, 秀夫
Citation	東京学芸大学紀要. 第4部門, 数学・自然科学, 56: 15-25
Issue Date	2004-08-02
URL	http://hdl.handle.net/2309/1639
Publisher	東京学芸大学紀要出版委員会
Rights	

Bulletin of Tokyo Gakugei University Sect. IV, **56**, pp. 15～25, 2004

Graded persisting activity of heterogeneous neuron ensembles subject to white noises

Hideo HASEGAWA*

Department of Physics

(Received for Publication; April 9, 2004)

HASEGAWA, H. : Graded persisting activity of heterogeneous neuron ensembles subject to white noises. Bull. Tokyo Gakugei Univ. Sec. **4**, 56 : 15 – 25 (2004) ISSN 0371-6813

Abstract

Effects of distractions such as noises and parameter heterogeneity have been studied on the firing activity of ensemble neurons, each of which is described by the extended Morris-Lecar model showing the graded persisting firings with the aid of an included Ca^{2+}-dependent cation current. Although the sustained activity of *single* neurons is rather robust in a sense that the activity is realized even in the presence of the distractions, the graded frequency of sustained firings is vulnerable to them. It has been shown, however, that the graded persisting activity of *ensemble* neurons becomes much robust to the distractions by the pooling (ensemble) effect. When the coupling is introduced, the synchronization of firings in ensemble neurons is enhanced, which is beneficial to firings of target neurons.

Key words : Graded persisting activity, Morris-Lecar model, Pooling effects

Department of Physics, Tokyo Gakugei University, Koganei-shi, Tokyo 184-8501, Japan.

1. Introduction

It has been reported that persistent activity of neurons is ubiquitous in living brains. Such persistent, stimulus-dependent activities are expected to be neuronal substrates of the short-term working memory (Brody, Rome and Kepecs, 2003). For example, in the prefrontal cortex of monkeys which are trained by short-term tasks, the persisting activity has been interpreted as a basis of working memory for a few seconds (Funahashi, Bruce and Goldman-Rakic, 1989; Miller, Erickson and Desimone, 1996; Romo, Hermandez, Lemus, Zainos and Brody, 2002). In the area I of goldfish hindbrain which controls the motor systems deriving the eye muscle, the persisting activity is interpreted as a short-term memory of the eye position that keeps the eye still between saccades (Pastor, Delacruz, and Baker, 1994; Seung, 1996; Aksay, Baker, Seung and Tank, 2000): oculomotor neurons are considered to integrate the velocity information from the eye movement, yielding information on the eye position.

One of the problems of the observed persisting activity is how to keep it for extended periods. Most models previously proposed are based on the recurrently coupled neural networks (Rosen, 1972; Cannon, Robinson and Shamma, 1983; Seung, Lee, Reis and Tank, 2000, Miller, Brody, Romo and Eang, 2003). These models may account for the observed property of the persistent activity. They have, however, a serious drawback requiring the fine tuning of the network-feedback gain within a tolerance of less than 1 % to stabilize the firing

* Phone:+81-42-329-7482; Fax: +81-42-329-7491; E-mail: hasegawa@u-gakugei.ac.jp

rate expressing stored information. If the overall gain of the network is slightly increased than the critical value, it leads to a divergent activity. On the other hand, if the gain is slightly decreased than the critical value, the state reduces to the stable fixed point without firings, losing the memory stored in the firing rate. Some homeostatic mechanisms such as an activity-dependent scaling of synaptic weights (Renart, Song and Wang, 2003) have been proposed for stabilizing the neural activity.

A new mechanism based on the bistability of neurons has been proposed (Rosen, 1972, Guigon, Dorizzi, Burnodand Schultz, 1995, Koulakov, Raghavachari, Kepec and Lisman, 2002). Two specific ways to realize bistable elements have been discussed: one by local excitation connections and the other by the voltage-dependent N-methyl-D-aspartate (NMDA) channel (Lisman, Fellous and Wang, 1998). Recurrent networks consisting of bistable elements have been shown to robustly operate even when the model parameters are not well tuned. It is, however, unclear whether the prediction of the bistable neuron is consistent with experimental data from neuronal integrators. For example, bistable neurons are reported to be absent in the goldfish oculomotor neurons which show the persistent activity (Pastor it *et al*., 1994; Aksay *et al*., 2000).

Quite recently, the graded persistent activity has been observed for *single*, *in vitro* neurons of the layer-V entorhinal cortex (EC) of rats (Egorov, Hamam, Fransein, Hasselmo and Alonso, 2002). The sustained firing rate of the neurons is shown to be proportional to the integral over time of its previous synaptic input. EC in the parahippocampal region is known to be associated with the working memory (Frank and Brown, 2003). It has been shown that EC neurons display persisting activity during the delay phase of delayed mach or non-match to sample memory task (Suzuki, Muller and Desimone, 1997, Young, Otto, Fox and Eichenbaum, 1997). A phenomenological rate-code model including multiple bistable dendrites has been proposed (Goldman, Levine, Major, Tank and Seung, 2003). It has been suggested that the calcium concentration is a plausible candidate for the observed parametric working memory (Egorov, Hamam, Fransein, Hasselmo and Alonso, 2002). Several conduction-based neuron models have been proposed based on Ca^{2+}-ion channel. Lowenstein and Sompolinksy (LS) (2003) have shown that by the diffusion of the non-linear dynamics of the calcium concentration in bistable dendrites, the wave-front of calcium propagates at a speed proportional to the synaptic inputs. When the Ca^{2+}-dependent cation is included in a neuron model described by the HH-type model (Shriki, Hansel and Sompolinsky, 2003), calculated firings show the behavior similar to the observed one. Teramae and Fukai (2003) have proposed detailed conductance-based models in which both L-type Ca channel and Ca^{2+}-dependent cation channel are taken into account.

It is interesting that in contrast to recurrent neural networks with bistable neurons, single neurons with bistable dendrites may store information in the form of the graded persisting activity. For a reliable performance of information storage, such single neurons are required to be robust against distractions such as noises and heterogeneity in neuron elements. It was reported (Mainen and Sejnowsky, 1995) that although firings of *in vitro* single neurons are precise, *in vitro* ones are quite unreliable due to noisy environment. This may suggest that noises might make the graded persisting activity of EC single neurons unreliable.

A small cluster of cortex generally consists of many similar neurons which include some degree of heterogeneity. Each neuron generates spikes which propagate to synapses exciting neurons in the next stage. It has been recognized that the population of neuron ensembles plays important roles in the information transmission. The population improves the reliability of response of noisy neurons. For example, the stochastic resonance in neuron ensembles is much effective than that of single neurons. An advantage of the synchronized activity is a large input on a target neuron.

From these considerations, we will make, in this paper, a theoretical study on the robustness of the parametric working memory, taking account of two factors: (1) neuron ensembles with (2) the heterogeneity and noises. In order to investigate the property of the persisting activity of an ensemble against noises and heterogeneity, we will perform simulations on ensemble neurons, each of which shows the persisting activity. We first develop a minimum, single neuron model, which is suitable for a simulation of ensemble neurons. The Morris-Lecar (ML) model, which was initially proposed for a barnacle giant muscle fiber, has been widely employed for a study on neuron dynamics (Morris and Lecar, 1981; Rinzel and Ermentrout, 1989). Although the ML model is the reduced, simplified model of the detailed HH model, it is more realistic than the integrate-and-fire model. A new variable for the calcium channel whose function depends on Ca^{2+}-ion concentration has been incorporated to the ML model. With the aid of Ca^{2+}-dependent current, a single ML neuron may

show the graded persisting activity.

The paper is organized as follows. The property of a single (extended) ML model is discussed in Sec. 2, where effects of noises and variations of model parameters are investigated. In Sec. 3, we have studied a neuron ensemble where each neuron is described by the extended ML model proposed in Sec. 2. Effects of noises and the heterogeneity of model parameters on the persisting activity have been investigated. The synchronization within neuron ensembles is also discussed. Conclusions and discussions are given in Sec. 4.

2. Dynamics of a single neuron

2. 1 Adopted model

We have adopted the extended ML neuron model for a single neuron, given by

$$C\frac{dv}{dt} = -I_{Ca} - I_K - I_{cat} - I_L + a + I(t) + \beta_v\,\xi(t), \quad (1)$$

$$\frac{dw}{dt} = \phi\left[\frac{w_o(v) - w}{\tau_w(v)}\right], \quad (2)$$

$$\frac{dz}{dt} = b + d\,[I(t) + \beta_z\,\eta(t)], \quad (3)$$

where

$$I_{Ca} = g_{\rm Ca} m_o(v)(v - v_{\rm Ca}), \quad (4)$$

$$I_K = g_{\rm K}\,w\,(v - v_{\rm K}), \quad (5)$$

$$I_{cat} = g_{\rm cat}\,z\,(v - v_{\rm cat}), \quad (6)$$

$$I_L = g_{\rm L}(v - v_{\rm L}), \quad (7)$$

with

$$m_o(v) = \frac{1}{2}\left[1 + tanh\left(\frac{v - v_1}{v_2}\right)\right], \quad (8)$$

$$w_o(v) = \frac{1}{2}\left[1 + tanh\left(\frac{v - v_3}{v_4}\right)\right], \quad (9)$$

$$\tau_w(v) = sech\left(\frac{v - v_3}{2v_4}\right). \quad (10)$$

The model given by Eqs. (1)-(10) takes into account the non-specified cation current (I_{cat}) besides Ca, K and leakage currents (I_{Ca}, I_K and I_L) which are included in the original ML model (Morris and Lecar, 1981; Rinzel and Ermentrout, 1989); v and w denote the fast membrane potential and the slow auxiliary variable, respectively; z expresses a new variable for the Ca^{2+}-ion concentration which is relevant to the cation channel. The variable z controls the conductance of the cation channel which yields the persistent parametric activity, as will be shown later. The equation of motion for z is assumed to be given by Eq. (3), where b and d stand for the drift velocity and the coefficient, respectively. Equation (3) may be justified, to some extent, by the model proposed by LS (Lowenstein and Sompolinsky, 2003), details being given in appendix A. The explicit form of an input current $I(t)$ will be shown shortly [Eq. (11)]. β_v and β_z express the strengths of independent white noises given by $\xi(t)$ and $\eta(t)$ with zero means and $<\xi(t)\,\xi(t')>=<\eta(t)\,\eta(t')>=\delta(t-t')$ and $<\xi(t)\,\eta(t')>=0$. In this study, we have adopted the following parameters: the capacitance is C=20, the reversal potentials of Ca, K, cation channels and leakage are $v_{\rm Ca}$=120, $v_{\rm K}$=−84, v_{cat}=40 and $v_{\rm L}$=−60, and the corresponding conductances are $g_{\rm Ca}$= 4, $g_{\rm K}$= 8, g_{cat}=1 and $g_{\rm L}$= 2: other parameters are v_1=−1.2, v_2=18, v_3=12 v_4=17.4, ϕ=0.0667 (Rinzel and Ermentrout, 1989), a=39.6, b=0, and d=0.0001: values of β_v and β_z will be shown shortly (in this paper, conductances are expressed in mS/cm^2, currents in $\mu A/cm^2$, voltages in mV, the time in ms and the capacitance in $\mu F/cm^2$). These parameter have not necessarily been chosen so as to reproduce observed data of EC (Egorov *et al.,* 2002).

2. 2 Calculated results

2. 2. 1 Property of the extended ML models

It is noted that our ML model with these parameters can start firings from the zero frequency when the parameter of a is varied for $a_1 \le a < a_2$ where the critical values are a_1=40 and a_2=116$\mu A/cm^2$ for b=0 and $I(t)$=0 [see Fig. 7.6 of Rinzel and Ermentrout, 1989]. Then our ML neuron belongs to the type-I neuron. Although the linearity of the a-f relation at $a \ge a_1$ is not perfect, it does not matter for our purpose discussing effects of distractions on the persisting activity.

We apply to our ML neuron, an input signal consisting of four pulses as given by

$$I(t) = \sum_{n=1}^{4} I_n(t) = A_i \sum_{n=1}^{4} c_n[\Theta(t - T_n^{(i)}) - \Theta(t - T_n^{(i)} - T_w)], \quad (11)$$

where A_i stands for the magnitude of a pulse, $T_n^{(i)}$=1000$n$ms (n: integer), T_w=200ms, c_n = 1 (−1) for n=1−3 (n=4), and $\Theta(t)$ is the Heaviside function. We have adopted A_i=20$\mu A/cm^2$ otherwise noticed.

Equations (1)-(11) have been solved by the fourth-order Runge-Kutta method with a time step of 0.01 ms, the initial condition being given by $v(0)$=−40, $w(0)$=0 and $z(0)$=0. Figure 1(a) shows time courses of v, w, and z when $I(t)$ given by Eq. (11) is applied to our ML neuron, $I(t)$ being depicted at the bottom of Fig. 1(a). The variable z is proportional to the integral on time of an input signal [Eq. (3)], and it shows a step-wise behavior: z is changed while an input pulse given by Eq. (11) is added and it stays at plateau values of z=0.02,

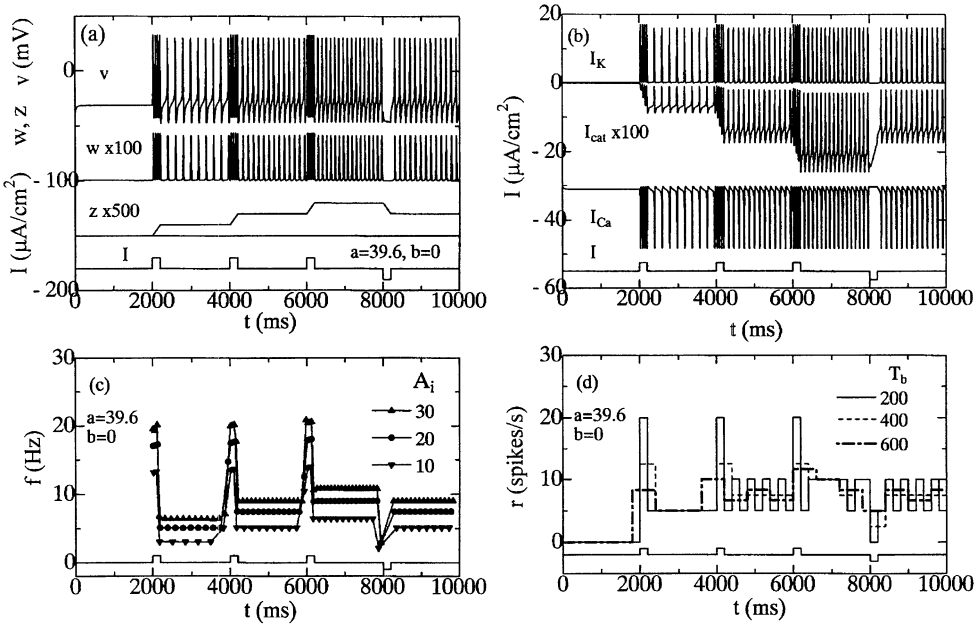

Figure 1 : Time courses of (a) v, w, z and I and (b) I_K, I_{cat} and I_{Ca} of a single ML neuron with A_i=20, a=39.6 and b=0; w, z and I are multiplied by factors of 100, 500, and 10, respectively, and are shifted downward by 100, 150, and 180, respectively; I_{cat} is multiplied by a factor of 100, and I_{Ca} is shifted downward by 30. (c) The time course of the frequency $f(t)$ which is the inverse of ISI, with A_i=10 (inverted triangles), 20 (circles) and 30 (triangles). (d) The histogram depicting the rate $r(t)$ of firings shown in (a) and (b) with the time bins of T_b= 200 (the solid curve), 400 (the dashed curve) and 600 (the chain curve).

0.04 and 0.06 between input pulses. Figure 1(b) shows time courses of currents of I_K, I_{Ca} and I_{cat}. It is noted that I_{Ca} and I_{cat} are inward (negative) currents while I_K is the outward (positive) one. When an input pulse is applied to a ML neuron, z is increased, which triggers a flow of I_{cat} and the oscillation of state variables. As z is furthermore increased by an injected pulse, the frequency of firing is increased.

This is more clearly seen by circles in Fig. 1(c), which shows the time-dependent frequency $f(t)$ defined as the inverse of the interspike interval (ISI):

$$f(t) = \frac{1}{T_n(t_n)} = \frac{1}{t_{n+1} - t_n}, \qquad \text{at } t = t_n \tag{12}$$

t_n being the nth firing time defined as the time when $v(t)$ crosses the threshold θ (-10 mV) from below. Neurons fire most strongly during the transient response to applied pulses and settle to a persistent firings which depend on the integral on time of the past inputs. An initial 200-ms depolarizing pulse results in a sustained firing of 5.1 Hz, and the second and third ones increase the frequency to 7.6 and 9.0 Hz, respectively, while a persisting firing backs to 7.6 Hz after the fourth hyperpolarizing pulse. We note that the firing frequency $f(t)$ is successively increased (decreased) when depolarizing (hyperpolarizing) pulses are applied, and that the frequency is constant with plateaus between applied pulses.

This trend is realized also in histogram in Fig. 1(d) expressing the firing rate $r(t)$ for various time bins of T_b=200 (solid curve), 400 (dashed curve) and 600 (chain curve). The rate with the small time bin of T_b=200 reproduces the transient behavior while impulses are applied, although it shows an oscillation at the plateau period. In contrast, for the rate with large T_b=600, the persisting firings are well explained while the transient firings are averaged out. When the magnitude of pulses A_i is increased (decreased), the value of $f(t)$ at plateau is increased (decreased), as shown by triangles (A_i=30) and inverted triangles (A_i=10) in Fig. 1(c). For example, the first depolarizing pulse with A_i=10, 20 and 30$\mu A/cm^2$ yields the sustained firing frequencies of 2.9, 5.1 and 6.5 Hz, respectively. Similarly, when the duration of pulses T_w is increased (decreased), the value of $f(t)$ at plateau is increased (decreased) (results are not shown). Calculated results are similar to those experimentally obtained for single EC neurons. (Egorov *et al.,* 2002).

Figures 2(a) and 2(b) show the v-w and z-v phase planes for firings shown in Fig. 1. For a comparison, nullclines of Eqs. (1) and (2) for a=39.6, b=0, z=0 and I=0 are shown by dashed and chain curves, respectively, which have a tangentially contact at (v,w)=(-29.6, 0.00846). The solid curve in Fig. 2(a) shows that the cycle starts from (v, w)=(-40, 0) and circles counter-clockwise almost independently of the z value. Figure 2(b) shows that between the plateau values of z=0.02, 0.04 and 0.06, v oscillates against z, and that v

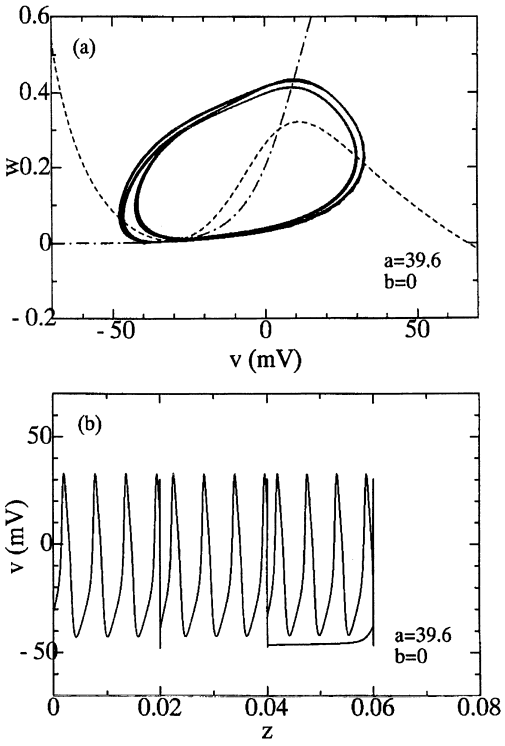

Figure 2: (a) The v-w and (b) z-v phase planes relevant to firings shown in Fig. 1; dashed and chain curves in (a) express nullclines of Eqs. (1) and (2) for A_i=20, a=39.6, b=0, z=0 and I=0.

changes vertically when z stays at these plateau values.

2. 2. 2 Effects of model parameters of *a* and *b*

We will investigate effects of parameters when their values are changed. Among many model parameters included in Eqs. (1)-(10), we have chosen a and b as the parameters to be changed because they are expected to play an important role in stabilizing the persisting firings. Figure 3(a) shows the time course of $f(t)$ for various a values of a=39, 39.6 and 41$\mu A/cm^2$ with b=0. For a=41, a neuron fires with f=5.2 Hz at t < 1000ms before the first pulse is applied, and firing frequencies after the second, third and fourth inputs are larger than those for a=39.6. In contrast, the firing frequency for a=39 is smaller than that for a=39.6.

Figure 3(b) shows $f(t)$ for various b values of b=−2, 0, and 2($\times 10^{-6}$) with a=39.6$\mu A/cm^2$. The result for b=0 is the same as that shown by circles in Fig. 1(c). For b=−2×10^{-6}, $f(t)$ between pulses is gradually decreased. For b=2×10^{-6}, in contrast, the frequency shows a positive drift.

2. 2. 3 Effects of white noises

Next we add white noises to our ML neuron. The time course of the frequency $f(t)$ when white noises of β_v=4 are added to the variable v in Eq. (1), is shown by dots in Fig. 3(c), where open circles express the result with no noises. Because of added noises, the frequency of persisting firings fluctuates. A similar behavior has been realized when noises are added to the variable z in Eq. (3), whose result for β_z= 2 is shown by dots in Fig. 3(d).

Figures 3(a)-3(d) show that a single neuron is rather robust

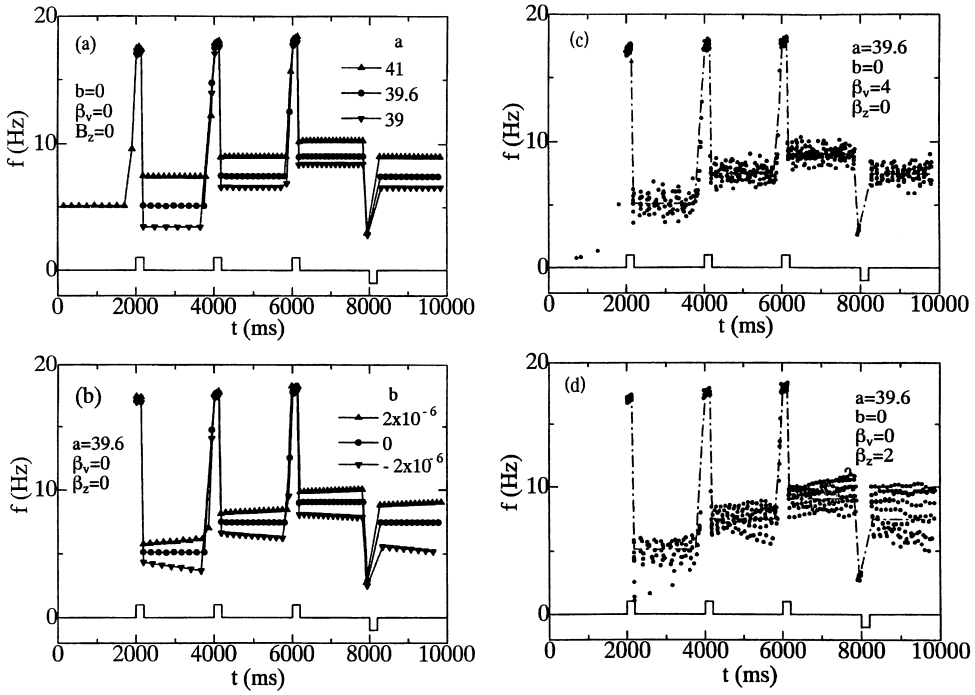

Figure 3: Time courses of the frequency $f(t)$ of a single ML neuron (a) for a=41 (triangles), 39.6 (circles) and 39 (inverted triangles) with b=0, β_v=0 and β_z=0, (b) for b=2×10^{-6}, 0 (circles) and −2×10^{-6} (inverted triangles) with a=39.6, β_v=0 and β_z=0, (c) for a=39.6, b=0, β_v=4, and β_z=0, and (d) for a=39.6, b=0, β_v=0, and β_z=2: an input signal is shown at bottoms. Results without noises (β_v=β_z=0) are shown by chain curves in (c) and (d), where simulation results are obtained by ten trials.

in a sense that the persisting firings are possible even when distraction are added. We note, however, that the frequency of the persisting firings is modified by distractions. The robustness is much improved in ensemble neurons by the pooling effect, as will be discussed in the following Se. 3.

3. Dynamics of neuron ensembles

3. 1 Adopted model

We have assumed that an ensemble consisting of N-unit ML neurons stores information from an applied signal of $I(t)$. Dynamics of an adopted, extended ML neuron model is given by

$$C\frac{dv_i}{dt} = g_{\rm Ca}m_o(v_i)(v_{\rm Ca}-v_i) + g_{\rm K}w_i(v_{\rm K}-v_i) + g_{\rm cat}\,z_i\,(v_{\rm cat}-v_i) + g_{\rm L}(v_{\rm L}-v_i) + a_i + I_i(t) + \beta_v\,\xi_i(t), \quad (13)$$

$$\frac{dw_i}{dt} = \phi\left[\frac{w_o(v_i)-w_i}{\tau_w(v_i)}\right], \quad (14)$$

$$\frac{dz_i}{dt} = b_i + d\,[I_i(t) + \beta_z\,\eta_i(t)], \quad (15)$$

$$I_i(t) = I(t) + \left(\frac{J}{N-1}\right)\sum_{j(\neq i)} G(v_j), \quad (i = 1\,\text{to}\,N) \quad (16)$$

where the sigmoidal function $G(v)$ is given by $G(v)=1/[1+\exp(v-\theta)/\alpha]$ with the coupling constant J, the threshold θ (=-10mV) and the width α(=1), self-coupling terms being excluded. β_v and β_z express the strengths of independent white noises of $\xi_i(t)$ and $\eta_i(t)$ with zero means and $<\xi_i(t)\,\xi_j(t')>=<\eta_i(t)\,\eta_j(t')>=\delta_{ij}\delta(t-t')$ and $<\xi_i(t)\,\eta_j(t')>=0$; other notations are the same as in Eqs.(1)-(10). The model parameters of a_i and b_i are assumed to be heterogeneous and their distributions obey the Gaussian distribution with

$$< a_i > = \epsilon, \quad (17)$$

$$< \delta a_i\,\delta a_j > = \lambda^2\,\delta_{ij}, \quad (18)$$

$$< b_i > = 0, \quad (19)$$

$$< b_i\,b_j > = \nu^2\,\delta_{ij}, \quad (20)$$

where $\delta a_i = a_i - \varepsilon$. We have adopted the same model parameters as for a single ML model discussed in Sec. 2.1 otherwise noticed.

3. 2 Calculated results

3. 2. 1 Homogeneous ensembles with no noises

When we perform simulations for 10-unit homogeneous ML neuron with no noises and no couplings (ε=39.6, λ=0, ν=0, β_v=0 and β_z=0, and J=0), we get the result in which time courses of state variables of v, w and z of all neurons in the ensemble are the same as that shown in Fig. 1(a) for a single ML neuron; $f(t)$ and $r(t)$ are also the same as those in Fig. 1(c) and 1(d). In the following, we will investigate effects of the heterogeneity and noises on the persisting activity in ML neuron ensembles.

3. 2. 2 Effects of heterogeneity

Raster in Fig. 4(a) shows firings of neuron ensembles when the heterogeneity of λ=1 is introduced to the parameter of a_i. Raster shows that due to the introduced heterogeneity,

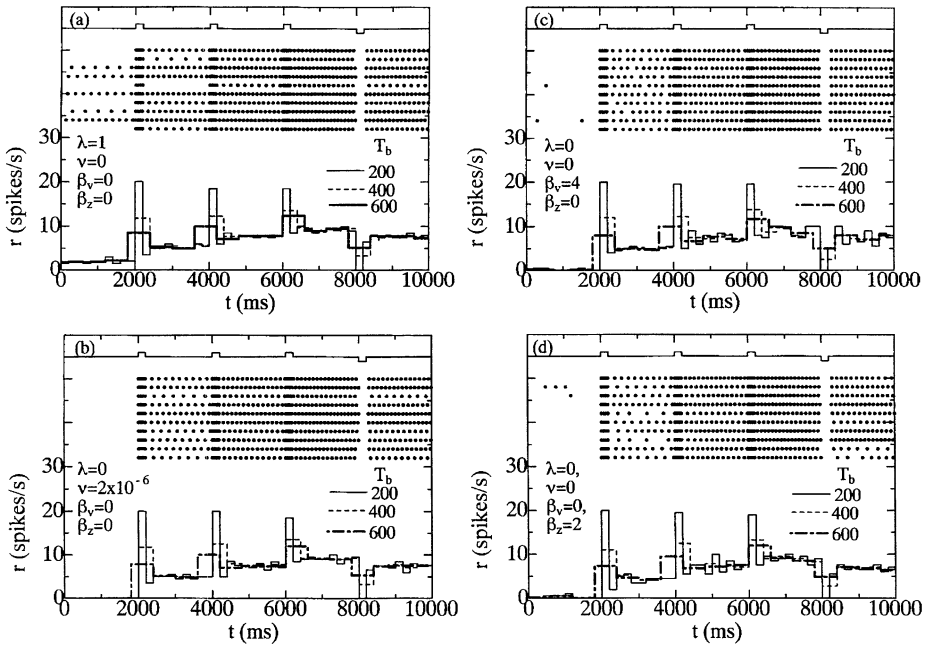

Figure 4: Rasters showing firings of 10-unit ML neuron ensembles and histograms expressing the firing rate $r(t)$ with time bins of T_b=200 (solid curves), 400 (dashed curves) and 600 (dot-dashed curves) for (a) λ=1, ν=0, β_v=0, β_z=0, (b) λ=0, ν=2×10^{-6}, β_v=0, β_z=0, (c) λ=0, ν=0, β_v=4$, β_z=0 and (d) λ=0, ν=0, β_v=0 β_z=2, with ε=39.6 and J=0, calculated by a single trial, an input signal being shown at bottoms.

firings of some neurons are increased while those of some neurons are decreased, compared to those in homogeneous neuron ensembles. For example, five neurons with large a_i fire before the first impulse is applied, which yields a finite firing rate at t < 1000ms. Nevertheless, the firing rate averaged over the ensemble is not so different from that of the homogeneous ensemble shown in Fig. 1(d).

Raster in Fig. 4(b) shows firings of an ensemble when the heterogeneity of $\nu=2\times10^{-6}$ is introduced to the parameter of b_i. The firing becomes irregular due to the introduced heterogeneity. However, the histogram of firing rate averaged over the ensemble shows a stable, persisting firing.

3. 2. 3 Effects of noises

We have added white noises to a ML neuron ensemble. Raster of Fig. 4(c) shows firing of the ensemble when noises with $\beta_v=4$ are added to the variable v. Because of added noises, firings of an ensemble become irregular. Despite added noises, a stable, persisting firing is realized as the averaged firing rate $r(t)$ shows,

When white noises of $\beta_z=2$ is added to the variable z, firings of an neuron ensemble become irregular, as raster in Fig. 4(d) shows. We note from the histogram that firings show a stable, persisting activity.

3. 2. 4 Effects of couplings

We have so far neglected the couplings among neurons ($J=0$) which are now taken into account. In order to examine the firing synchrony in an ensemble, we consider the quantity given by

$$R(t) = \frac{1}{N^2}\sum_i\sum_j < [v_i(t) - v_j(t)]^2 >, \tag{21}$$

which is zero in the completely synchronized state. By using a proper normalization factor of $R_0(t)=2(1-1/N)\gamma(t)$ which expresses the $R(t)$ value for an asynchronous state, we define the *synchronization ratio* given by (Hasegawa, 2003a, 2003b)

$$S(t) = 1 - \frac{R(t)}{R_0(t)} = \frac{\zeta(t)}{\gamma(t)}, \tag{22}$$

where

$$\zeta(t) = \frac{1}{N(N-1)}\sum_i\sum_{j(\neq i)} < \delta v_i(t)\,\delta v_j(t) >, \tag{23}$$

$$\gamma(t) = \frac{1}{N}\sum_i < \delta v_i(t)^2 >, \tag{24}$$

with $\delta v_i(t)=v_i(t)-<v_i(t)>$. It is easy to see that $S(t)$ is 1 and 0 for the completely synchronous and asynchronous states, respectively.

The lower frame of Figs. 5(a) shows the time course of the frequency $f(t)$ calculated for an ensemble with the heterogeneity of $\lambda=1$ and no couplings ($J=0$) by 100 trials. This should be compared to the histogram for the rate shown in Fig. 4(a), which has been calculated by a single trial. The middle frame of Fig. 5(a) expresses the synchronization ratio $S(t)$, which is vanishing because of the heterogeneity (with no couplings). Lower frames of Figs. 5(b), 5(c) and 5(d) show $f(t)$ for introduced couplings of $J=20$, 40 and 60, respectively. The distribution of $f(t)$ for $J=20$ become wider than that for $J=0$. This may be understood as follows. When any neuron with a large a_i fires, its spike propagates through couplings and induces firings in other neurons of an ensemble. When the coupling is furthermore increased, however, the distribution in $f(t)$ is reduced as the lower frame of Fig. 5(d) for $J=60$ shows. In contrast, the synchronization ratio $S(t)$ shown in the middle frames of Fig. 5(b), (c) and (d) is gradually increased as J is increased. It is interesting to note that the synchronization ratio is enhanced by transient impulses, and that $S(t)$ is gradually developed as more impulses are applied.

Figures 6(a)-6(d) show similar plots of $f(t)$ and $S(t)$ for ensembles with various couplings subject to noises of $\beta_v=4$, calculated by 100 trials. Lower and middle frames of Fig. 6(a) show that for $J=0$, $f(t)$ has a wide distribution and $S(t)$ is zero due to noises. When the coupling is introduced, the distribution of $f(t)$ is once increased for $J=20$, but reduced for stronger $J=40$ and 60 while the synchronization ratio $S(t)$ is monotonously increased as increasing J. The J dependence of $f(t)$ and $S(t)$ in Figs. 6(a)-6(d) is the same as that in Figs. 5(a)-5(d).

4. Conclusion and Discussion

In this paper, we have first proposed a minimum, conductance-based model showing the graded persisting activity by incorporating a calcium channel (Lowenstein and Sompolinsky, 2003) to the ML model (Morrris and Lecar, 1981; Rinzel and Ermentrout, 1989). Then, by employing the extended ML model, we have studied effects of distractions such as noises and the heterogeneity in model parameters on the persisting activity of single and ensemble neurons. The activity of single ML neurons is vulnerable because the frequency of persisting firings is modified by the distractions. In particular, even a small b ($=2\times10^{-6}$) yields a slow drift in the sustained frequency [Fig. 3(b)]. This is partly due to the fact that the value of the variable z is very small (~0-0.06) compared to those of v and w. As discussed in appendix A, a vanishing of the drift

requires $b=0$, which is realized when parameters of c_1, c_2 and c_3 satisfy the condition given by $c_2=(c_1+c_3)/2$ [Eq. (A13)]. This condition may be relaxed when a given neuron has multidendritic branches, for which b is expressed by $b=<b_m>_m$, b_m being the b term relevant to the mth dendrite and $<>_m$ the average over multidendrites. The averaging over multidendrites is expected to yield $b=0$ for single neurons. Even if b remains finite (but small), the drift of the sustained frequency may vanish in neuron ensembles [Fig. 4(b)] because of the pooling (ensemble) effect which is widely observed in various neuronal functions. Although we have made simulations only for several typical sets of parameter values, they have shown that the graded persisting activity of a neuron ensemble becomes more robust against distractions than that of a single neuron again by the pooling effect

The temporally correlated neuronal activity, the synchrony, has been considered to be important to various neuronal processing such as perception (Gray and Singer 1989, Gray, König, Engel and Singer, 1989) and attention (Steinmetz et al. 2000, Fries, Reynolds, Rorie and Desimone 2001). Recently

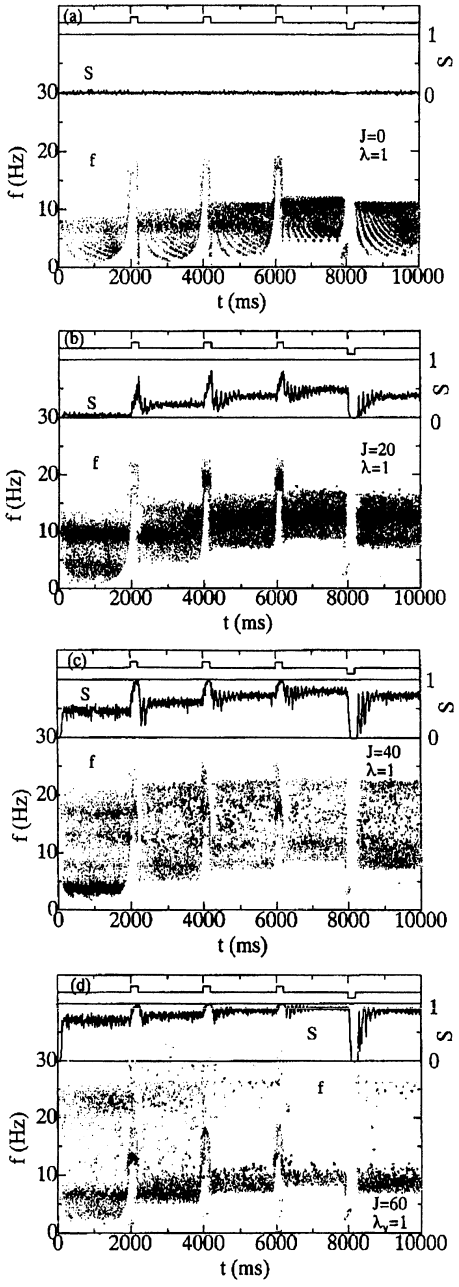

Figure 5: Time courses of the frequency $f(t)$ (lower frames) and the synchronization ratio $S(t)$ (middle frames) of heterogeneous ML neuron ensembles for (a) $J=0$, (b) $J=20$, (c) $J=40$ and (d) $J=60$, with $\lambda=1$, $\beta_v=0$, $\varepsilon=39.6$ and $\beta_z=0$, calculated by 100 trials; an input signal is shown in upper frames, and left and right ordinates are for $f(t)$ and $S(t)$, respectively.

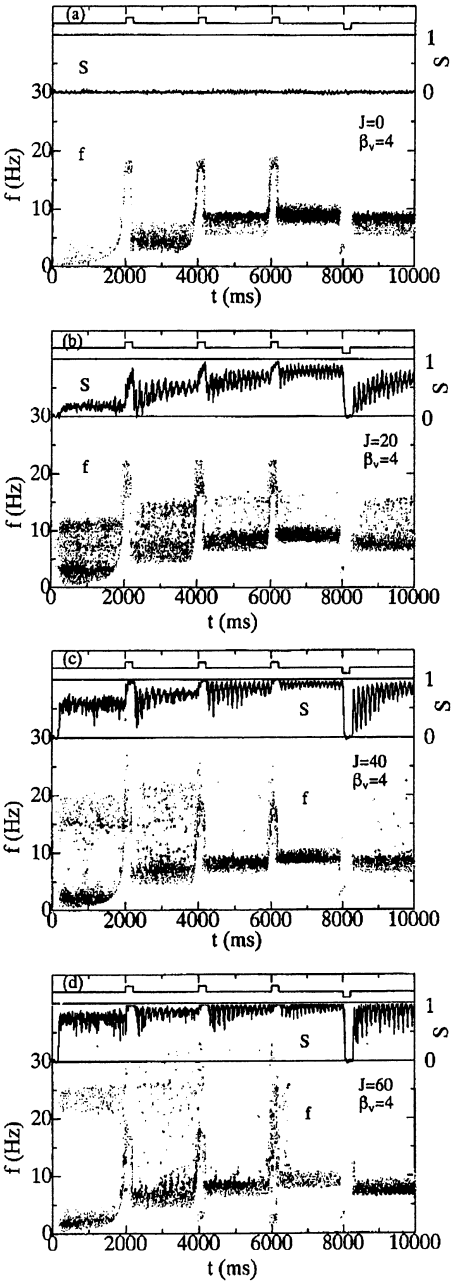

Figure 6: Time courses of the frequency $f(t)$ (lower frames) and the synchronization ratio $S(t)$ (middle frames) of noisy ML neuron ensembles for (a) $J=0$, (b) $J=20$, (c) $J=40$ and (d) $J=60$, with $\beta_v=4$, $\lambda=0$, $\varepsilon=39.6$ and $\beta_z=0$, calculated by 100 trials; an input signal is shown in upper frames, and left and right ordinates are for $f(t)$ and $S(t)$, respectively.

the temporal structure in neuronal activity during working memory has been observed in parietal cortex of monkey (Pesaran, Pezaris, Sahani, Mitra and Andersen, 2002). Our calculations have shown that couplings among neurons enhance the synchrony, which is expected to be beneficial to firings of target neurons. It is necessary to make more detailed study on the interaction and synchrony in neuron ensembles with the persisting activity. Our calculations in this study have been based on direct simulations. We are under consideration to apply, to the ML model, a semi-analytical dynamical mean-field theory which was successfully applied to large-scale neuron ensembles described by FitzHugh-Nagumo and Hodgkin-Huxley models (Hasegawa, 2003a, 2003b).

Acknowledgements

This work is partly supported by a Grant-in-Aid for Scientific Research from the Japanese Ministry of Education, Culture, Sports, Science and Technology.

Appendix A. Derivation of Eq.(3)

Assuming a long, linear dendrite for $x \in [-L, L]$, Lowenstein and Sompolinsky (LS) (2003) have shown that the Ca^{2+}-dependent cation current is given by

$$I_{cat}(t) = g_{cat}\, z(t)\, (v - v_{cat}), \tag{A1}$$

with the spatially-summed Ca^{2+} concentration of $z(t)$ given by

$$z(t) = \int_{-L}^{L} dx\; c(x,t), \tag{A2}$$

where $c(z, t)$ stands for the space- and time-dependent Ca^{2+} concentration satisfying the partial differential equation given by

$$\frac{\partial c(x,t)}{\partial t} = h(c(x,t)) + D\frac{\partial^2 c(x,t)}{\partial x^2} + k(c(x,t))\, I(t). \tag{A3}$$

Here $h(c)=-K(c-c_1)(c-_2)(c-c_3)$ and $k(c)=(K/2)(c_3-c_1)(c-c_1)(c-c_3)$ with $c_1 < c_2 < c_3$, $I(t)$ denotes an input signal, D the diffusion constant and K the positive coefficient. The functional form of $h(c)$ shows that the state is bistable at $c=c_1$ and $c=c_3$ but unstable at $c=c_2$. LS have shown that the solution of Eq. (A3) for the boundary condition of $c(-L,t)=u_3$ and $c(L,t)=u_1$, is given by

$$c(x,t) = c_2 + \left(\frac{c_3 - c_1}{2}\right)\, tanh\left[\frac{x - P(t)}{\lambda}\right], \tag{A4}$$

with

$$P(t) = P(0) + ut + s\int_0^t dt'\; I(t'), \tag{A5}$$

where

$$\lambda = \left(\frac{2}{c_3 - c_1}\right)\sqrt{\frac{2D}{K}}, \tag{A6}$$

$$u = \sqrt{2DK}\left[c_2 - \left(\frac{c_1 + c_3}{2}\right)\right], \tag{A7}$$

$$s = (c_3 - c_1)\sqrt{2DK}. \tag{A8}$$

Equations (A4)-(A8) imply that the position of the front of Ca^{2+}-concentration moves with the velocity of u, and it is proportional to the integral of the input signal $I(t)$. By using Eqs. (A1)-(A8), we get

$$\frac{dz}{dt} = \left(\frac{c_3 - c_1}{2}\right)\left(tanh\left[\frac{-L - P(t)}{\lambda}\right] - tanh\left[\frac{L - P(t)}{\lambda}\right]\right)\frac{dP(t)}{dt}, \tag{A9}$$

$$\simeq b + d\, I(t), \tag{A10}$$

with

$$b = (c_3 - c_1)\, u, \tag{A11}$$

$$d = (c_3 - c_1)\, s, \tag{A12}$$

leading to Eq. (3). Equations (A8) and (A11) show that b does not vanish unless parameters of c_1, c_2 and c_3 satisfy the condition:

$$c_2 = \frac{c_1 + c_3}{2}, \tag{A13}$$

although LS adopted $b=0$ assuming the condition given by Eq. (A13).

For a single neuron with M-unit multiple dendritic branches where the same signal is applied to all synapses, the equation of motion for the averaged variable of $z=\sum_{m=1}^{M} z_m \equiv <z_m>_m$ is again given by Eq. (A10) but with $b=<b_m>_m$ and $d=<d_m>_m$ where z_m, b_m and d_m denote quantities relevant to the mth dendrite.

References

Aksay E., Baker R., Seung H. S., and Tank D. W. (2000). Anatomy and discharge properties of pre-motor neurons in the Goldfish medulla that have eye-position signals during fixations. *Journal of Neurophysiology,* **84**, 1035-1049.

Brody C. D., Rome R., and Kepecs A. (2003). Basic mechanisms for graded persistent activity: discrete attractors, continuous attractors, and dynamic representations. *Current Opinion on Neurobiology,* **13**, 204-211; related references therein.

Camperi M. and Wang X. J. (1998). A model of visuospatial

working memory in prefrontal cortex: recurrent network and cellular bistability. *Journal of Computational Neuroscience,* **5**, 383-405.

Cannon S. C., Robinson D. A.. and Shamma S.(1983). A proposed neural network for the integrator of the oculomotor systems. *Biological Cybernetics,* **49**, 127-136.

Egorov A. V., Hamam B. N., Fransein E., Hasselmo M. E., and Alonso A. A. (2002). Graded persistent activity in entorhinal cortex neurons. *Nature,* **420**, 173-178.

Frank L. M. and Brown E. N. (2003). Persistent activity and memory in the entorhinal cortex. *Trends in Neurosciences,* **26**, 400-401.

Fries P., Reynolds J. H., Rorie A. H. and Desimone R., (2001). Modulation of oscillatory neuronal synchronization by selective visual attention. *Science,* **291**, 1560-1563.

Funahashi S., Bruce C. J., and Goldman-Rakic P. S. (1989). Mneumonic coding of visual space in the monkeys dorsolateral cortex. *Journal of Neurophysiology,* **61**, 331-349.

Goldman M. S., Levine J. H., Major G., Tank D. W. and Seung H. S. (2003). Robust persistent neural activity in a model integrator with multiple hysteretic dendrites per neuron. *Cerebral Cortex,* **13**, 1185-1195.

Gray C. M., König P., Engel A. K. and Singer W. (1989). Oscillatory responses in cat visual cortex exhibit inter-columnar synchronization which reflects global stimulus properties. *Nature,* **338**, 334-337.

Gray C. M. and Singer W. (1989). Stimulus-specific neuronal oscillations in orientation columns of cat visual cortex. *Proceedings of National Academy of Sciences of the United State of America,* **86**, 1698-1702.

Guigon E., Dorizzi B., Burnod Y. and Schultz W. (1995). Neural correlates of learning in the prefrontal cortex of monkey. *Cerebrum Cortex,* **2**, 135-147.

Hasegawa H., (2003a) Dynamical mean-field theory of spiking neuron ensembles: Response to a spike with independent noises. *Physical Review E,* **67**, 041903.1-041903.19.

Hasegawa H., (2003b) Dynamical mean-field theory of noisy spiking neuron ensembles: Application to Hodgkin-Huxley model. *Physical Review E,* **68**, 041909. 1-041909.13.

Koulakov A. A., Raghavachari S., Kepec A., and Lisman J. E. (2002). Model for a robust neural integrator. *Nature Neuroscience,* **5**, 775-782.

Lisman J. E., Fellous J. M., and Wang X. J. (1998). A role for NMDA-receptor channels in working memory. *Nature Neuroscience,* **1**, 273-275.

Lowenstein Y. and H. Sompolinsky (2003). Temporal integration by calcium dynamics in a model neuron. *Nature Neuroscience,* **6**, 961-967

Mainen Z. F., and Sejnowsky T. J. (1995). Reliability of spike timing in neocortical neurons. *Science,* **268**, 1503-1506.

Miller E. K., Erickson C. A., and Desimone R. (1996). Neural mechanisms of visual working memory in prefrontal cortex of macaque. *The Journal of Neuroscience,* **16**, 5154-5167.

Miller P., Brody C. D., Romo R. and Wang X. (2003). A recurrent network model of somatosensory parametric working memory in the prefrontal cortex, *Cerebrum Cortex,* **13**, 1208-1218

Morris C. and Lecar H. (1981). Voltage oscillations in the barnacle giant muscle fiber. *Biophysics* **35**, 193-213.

Pastor A. M., Delacruz R. R., and Baker R. (1994). Eye position and eye velocity integrators reside in separate brain-stem nuclei. *Proceedings of National Academy of Sciences of the United State of America,* **91**, 807-811.

Pesaran B., Pezaris J. S., Sahani M., Mitra P. P. and Andersen R. A. (2002). Temporal structure in neuronal activity during working memory in macaque parietal cortex. *Nature Neuroscience,* **5**, 805-811.

Renart A., Song P. and Wang X. (2003). Robust spatial working memory through homeostatic synaptic scaling in heterogeneous cortical networks. *Neuron,* **38**, 473-485.

Rinzel J. R. and Ermentrout G. (1989). Analysis of neural excitability and oscillation. In C. Koch and I. Segev, (Eds.), *Methods in neural modeling* (pp251-291), MIT press, Cambridge, MA.

Romo R., Hermandez A., Lemus L., Zainos A., and Brody C. D. (2002). Neuronal correlates of decision-making in secondary somatosensory cortex. *Nature Neuroscience,* **5**, 1217-1225.

Rosen M. (1972). A theoretical neural integrator. *IEEE Transactions on Biomedical Engineering,* **19**, 362-367.

Seung H. S. (1996). How the brain keeps the eyes still. *Proceedings of National Academy of Sciences of the United State of America,* **93**, 13339-13344.

Seung H. S., Lee D. D., Reis B. Y., and Tank D. W. (2000). The autapse: A simple illustration of short-term analog memory storage by tuned synaptic feedback. *Journal of Computational Neuroscience,* **9**, 171-185.

Shriki O., Hansel D., and Sompolinsky H. (2003). Rate

models for conductance-based cortical neuronal networks. *Neural Computation,* **15**, 1809-1841.

Steinmetz P. N., Roy A., Fitzgerald P. J., Hsiao S. S., Johnson K. O. and Niebur E. (2000). Attention modulates synchronized neuronal firing in primate somatosensory cortex. *Nature,* **404**, 187-190.

Suzuki W. A., Miller E. K. and Desimone R. (1997). Object and place memory in the macaque entorhinal cortex. *Journal of Neurophysiology,* **78**, 1062-1081.

Taramae J. and Fukai T. (2003). A novel cellar mechanism for parametric working memory in a model neuron.

Young B. J., Otto T., Fox G. D. and Eichenbaum H. (1997). Memory representation within parahippocampal region. *The Journal of Neuroscience* **17**, 5183-5195.